Band Engineering of Dirac Surface States in Topological-Insulator-Based van der Waals Heterostructures

Cui-Zu Chang,[1,2,*] Peizhe Tang,[1] Xiao Feng,[1,2] Kang Li,[2] Xu-Cun Ma,[1,4] Wenhui Duan,[1,3,4,†] Ke He,[1,4,‡] and Qi-Kun Xue[1,2,4]

[1]*State Key Laboratory of Low-Dimensional Quantum Physics, Department of Physics, Tsinghua University, Beijing 100084, China*

[2]*Beijing National Laboratory for Condensed Matter Physics, Institute of Physics, Chinese Academy of Sciences, Beijing 100190, China*

[3]*Institute of Advanced Study, Tsinghua University, Beijing 100084, China*

[4]*Collaborative Innovation Center of Quantum Matter, Beijing 100084, China*

(Received 15 April 2015; revised manuscript received 4 July 2015; published 23 September 2015)

The existence of a gapless Dirac surface band of a three dimensional (3D) topological insulator (TI) is guaranteed by the nontrivial topological character of the bulk band, yet the surface band dispersion is mainly determined by the environment near the surface. In this *Letter*, through *in situ* angle-resolved photoemission spectroscopy and first-principles calculation on 3D TI-based van der Waals heterostructures, we demonstrate that one can engineer the surface band structures of 3D TIs by surface modifications without destroying their topological nontrivial property. The result provides an accessible method to independently control the surface and bulk electronic structures of 3D TIs, and sheds light on designing artificial topological materials for electronic and spintronic purposes.

DOI: 10.1103/PhysRevLett.115.136801 PACS numbers: 73.20.At, 73.25.+i, 75.70.Tj

A topological insulator (TI) has conducting surface states (SSs) protected by the nontrivial topological property of its insulating bulk bands [1,2]. The topological SSs of TIs have Dirac-cone-shaped band structure and are spin-momentum locked [3–6]. Exotic physical phenomena such as Majorana fermions [2] and the quantum anomalous Hall effect [7–9] have been proposed based on TIs, which bring the materials tremendous application potential in future spintronics and fault-tolerant quantum computation. Bi_2Se_3, Bi_2Te_3, and Sb_2Te_3 are the most-studied 3D TIs by virtue of their simple composition and single Dirac cone band structure [3–6]. To realize various quantum phenomena and applications of TIs, one needs to be able to engineer the band structures of Dirac SSs (DSSs) while keeping bulk insulating properties. However, for a homogeneous TI material its bulk and surface properties are interdependent; the efforts of optimizing one will usually deteriorate the other. For example, to tune the Fermi level of Sb_2Te_3 into the bulk gap, one can dope Bi in it. This would inevitably push the Dirac point (DP) below the valence band maximum, burying its exotic electronic properties [10,11]. Thus the flexible and stable tuning of the properties of SSs and bulk bands of 3D TIs is a prerequisite for obtaining appropriate TIs for different purposes.

In fact, the unique character of TI provides a solution to the problem [1,2]. Although the existence of the DSSs of a TI is guaranteed by the topological character of the bulk band, the specific band structure of the DSSs is mainly determined by the potential landscape near the surface. Thus, just like conventional SSs, the band structure of topological DSS can be modulated by surface modifications but will still be protected as long as time reversal symmetry is kept [12].

Inspired by this idea, we use molecular beam epitaxy (MBE) to deposit different van der Waals cover layers [e.g., one quintuple layer (QL) TI film (TI_c) or one bilayer (BL) Bi(111)] on the other kind of 3D TI films (TI_b), as shown in Fig. 1. Combined with angle-resolved photoemission spectroscopy (ARPES) measurements and density functional theory (DFT) calculations, we find that the SS bands can be engineered by heteroepitaxy of the other material. For the heterostructures deposited by one QL TI_c, the energy dispersion of the SS and the surface carrier type are determined by the cover layer. While, for Bi_2Se_3 thin films covered by one BL Bi(111), the band crossing of the spin-polarized states originated from the large Rashba splitting of Bi BL coexists with the DSS of Bi_2Se_3; and owing to the strong surface hybridization, the energy dispersion and Fermi surface (FS) of DSS have been strongly modified. This work elucidates that depositing heterogeneous cover layers on TI thin films is a feasible approach to engineer the topological DSS, which allows us to achieve ideal TIs.

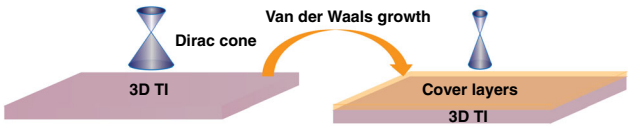

FIG. 1 (color online). Schematics of the van der Waals growth of cover layers on 3D topological insulator thin films.

Single crystal TI_b films were grown on a graphene terminated 6H-silicon carbide (0001) substrate [13]. When a thick TI_b film is grown, 1 QL TI_c was deposited onto it. During the growth of 1 QL TI_c, the substrate temperature is slightly lower (~10°C) than the growth temperature of thick TI_b films to minimize the possible intermixing. For 1 BL Bi(111) on a 20 QL Bi_2Se_3 heterostructure, a 1 BL Bi(111) film is deposited on the thick TI_b films at room temperature and annealed at 200°C for 1 h [14].

1 QL TI_c film on TI_b.—Figure 2(a) show the band dispersions and corresponding momentum distribution curves (MDC) along the $\bar{\Gamma}$-$\bar{K}$ direction for 10 QL Bi_2Se_3 films measured at $T \sim 150$ K, respectively. Topological DSS and quantum well states of the conduction band are clearly observed and the DP is located at ~395 meV below the Fermi level (E_F), much lower than that of the thick Bi_2Se_3 films [Fig. 4(a)]. As previously reported for a 1 QL Bi_2Te_3 film grown on a Si(111) substrate, the SSs open a gap at the DP position [15]. However, when 1 QL Bi_2Te_3 is on top of 10 QL Bi_2Se_3 films, a single gapless Dirac cone is observed in the bulk band gap. The surface band dispersion near DP is almost identical to the DSS of slightly hole-doped 3D TI Bi_2Te_3 films [16], but the DP is faintly lifted out of the bulk valence bands, as shown in Fig. 2(b). The significant change of DSS band dispersion from that of Bi_2Se_3 to that of Bi_2Te_3, instead of coexistence, indicates that 1 QL Bi_2Te_3 basically covers the whole surface of 10 QL Bi_2Se_3. This ultrathin 1 QL Bi_2Te_3 changes the DSS of 10 QL Bi_2Se_3, and makes the 1 QL Bi_2Te_3/10 QL Bi_2Se_3 heterostructure show DSS of the Bi_2Te_3 characteristic. This observation can be understood by TI band theory [1,2], where 3D Bi_2Te_3 shares the same bulk nontrivial Z_2 number with 3D Bi_2Se_3, while the 1 QL Bi_2Te_3 cover layer does not change the bulk nontrivial Z_2 topology of 10 QL Bi_2Se_3, resulting in a DSS, which is mainly determined by the surface Hamiltonian. Figure 2(c) is the band dispersion and the corresponding MDC along the $\bar{\Gamma}$-$\bar{K}$ direction for 10 QL Sb_2Te_3, respectively. The DSS is clearly observed and DP is located at +45 meV above the E_F, indicating p-type carriers. When 1 QL Bi_2Te_3 is covered on 10 QL Sb_2Te_3, a single gapless Dirac cone is observed in the bulk band gap below the E_F, while the surface band dispersion near DP is similar to the DSS of hole-doped 3D TI Bi_2Te_3 films [15], as shown in Fig. 2(d). This prominent DSS induced by 1 QL Bi_2Te_3 from Sb_2Te_3 to Bi_2Te_3 is also reasonable due to their same bulk Z_2 topology.

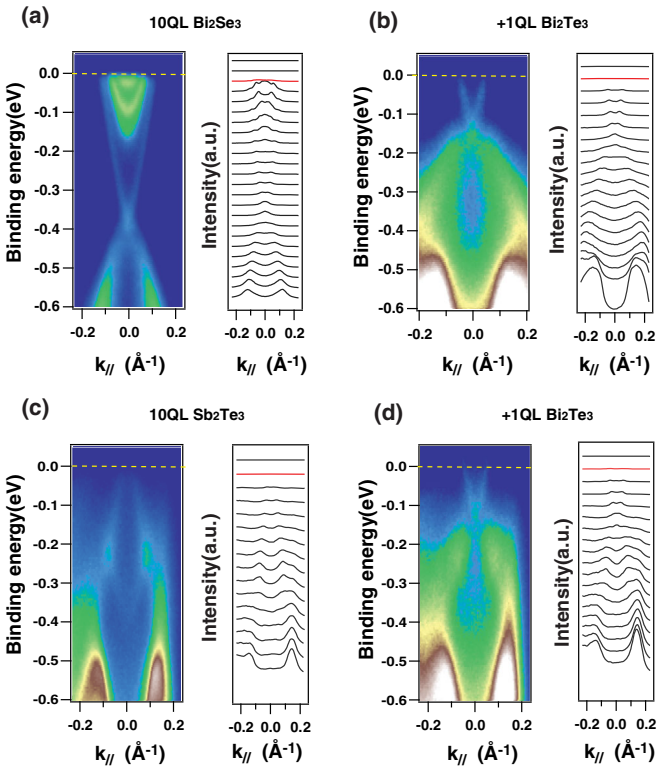

FIG. 2 (color online). Dirac surface states engineering in 3D TI films when another 1 QL TI film is deposited on the surface. ARPES band structures and corresponding momentum distribution curves (MDCs) of (a) 10 QL Bi_2Se_3, (b) 1 QL Bi_2Te_3/10 QL Bi_2Se_3, (c) 10 QL Sb_2Te_3, and (d) 1 QL Bi_2Te_3/10 QL Sb_2Te_3. All the spectra were taken along the $\bar{\Gamma}$-$\bar{K}$ direction at $T \sim 150$ K.

To further confirm the ARPES results, we carried out *ab initio* DFT calculations to study the electronic structures of 1 QL TI_c/6QL TI_b heterostructure, such as 1 QL Sb_2Te_3 on 6 QL Bi_2Te_3 thin films and vice versa. The calculated band structures are shown in Fig. 3, where the red shows the contributions from the top cover layer. Compared with the pristine 6 QL Bi_2Te_3 thin film [Fig. 3(a)], the DSS of the heterostructure still exists and is mainly contributed to by a covered 1 QL Sb_2Te_3 thin film, showing the characteristic of the Sb_2Te_3 SS [Fig. 3(b)], meanwhile the quantum well states contributed by Bi_2Te_3 are also retained in this heterostructure. Similar phenomena are also observed in 1 QL Bi_2Te_3 on 6 QL Sb_2Te_3 thin films, whose DSS has been engineered by the top cover layer only of 1 QL Bi_2Te_3 [Figs. 3(c) and 3(d)], consistent with the experimental observation [Figs. 2(c) and 2(d)]. These results suggest that the heterogeneous growth of other heterotype TI_c that also belong to the Bi_2Se_3 family cannot change the bulk band nontrivial Z_2 topology, while it can efficiently modulate the DSS. This artificial band engineering approach guides us to design an ideal TI heterostructure—with maintenance of high surface mobility and simultaneously tunable carrier type, but insulating bulk states—as an excellent platform for the further study.

1 BL Bi(111) on Bi_2Se_3.—Besides the heterostructure between 1 QL TI_c and 3D TI_b, 1 BL Bi(111) films have also been tried to deposit on 3D TI films to form a heterostructure. The electronic band dispersions of pristine and 1 BL Bi(111) covered 20 QL Bi_2Se_3 thin films measured by *in situ* ARPES along the $\bar{\Gamma}$-$\bar{K}$ direction are shown in Figs. 4(a) and 4(b), respectively. Two bands with nearly linear dispersion cross each other at the $\bar{\Gamma}$ point,

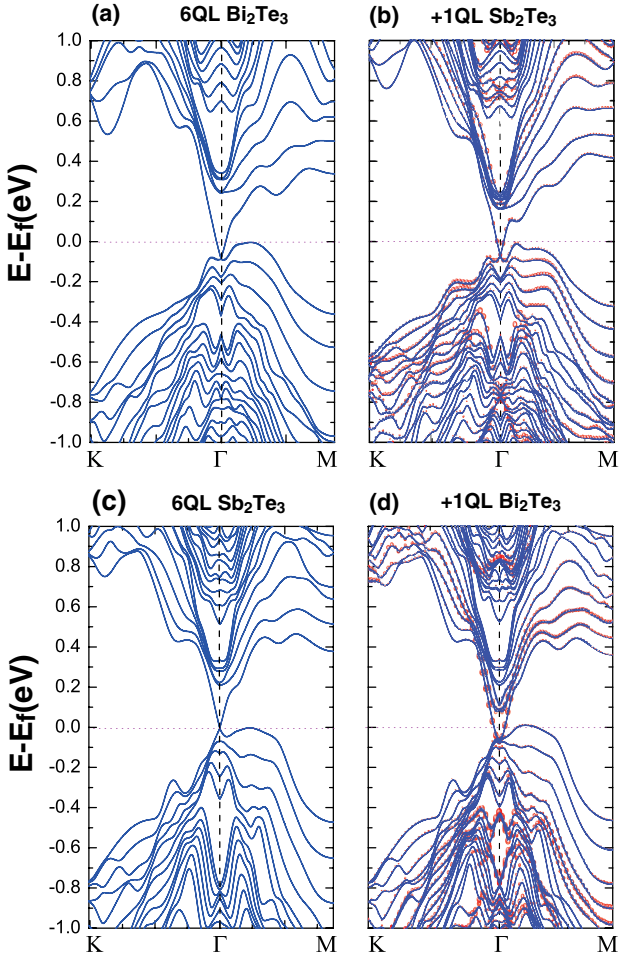

FIG. 3 (color online). First-principles calculations for the artificially engineered Dirac surface states. The DFT band structures of (a) 6 QL Bi_2Te_3, (b) 1 QL Sb_2Te_3/6 QL Bi_2Te_3, (c) 6 QL Sb_2Te_3, and (d) 1 QL Bi_2Te_3/6 QL Sb_2Te_3. The red solid and hollow dots in (b) and (d) show the bands induced by the topmost layer 1 QL Sb_2Te_3 or Bi_2Te_3.

forming a Dirac cone in pristine 20 QL Bi_2Se_3 thin films. The bulk conduction band can be observed and the DP is embedded in −190 meV below the E_F. Intriguingly, this situation will be changed when 1 BL Bi(111) is deposited on the surface. Besides the topological DSSs of 20 QL Bi_2Se_3, an additional pair of large Rashba-type splitting bands dispersing downwards from ± 0.08 Å^{-1} at the FS is raised. The brighter two bands' crossing state indicates the DP of the bottom 20 QL Bi_2Se_3, which is located at −300 meV below the E_F, it indicates that 1 BL Bi(111) introduces some electrons into 20 QL Bi_2Se_3. The additional bright state feature crossed by the Rashba-type subbands emerge in the vicinity of the top cone of DSS [16–18]. Because of BL Bi(111), there is a distinct modification for the band dispersions of DSS, which is extensively analyzed in detail in the corresponding MDC. For the constant energy contours of bands in 1 BL Bi(111)/20 QL Bi_2Se_3, shown in Fig. 4(c), the strong hexagonal warping effect can be observed in the FS of the outermost band, which shows snowflake shape and nests together with the FS of TI's surface state, as well as a slight warping effect. On the contrary, the inner FS of the Rashba-split subbands shows a nearly circular shape, which has a Rashba-like nondegenerate spin texture [19].

The 1 BL Bi(111) layer changes the band dispersion of the DSS contributed by the substrate of Bi_2Se_3, the most prominent feature is a tunability of the DSS slope near DP,

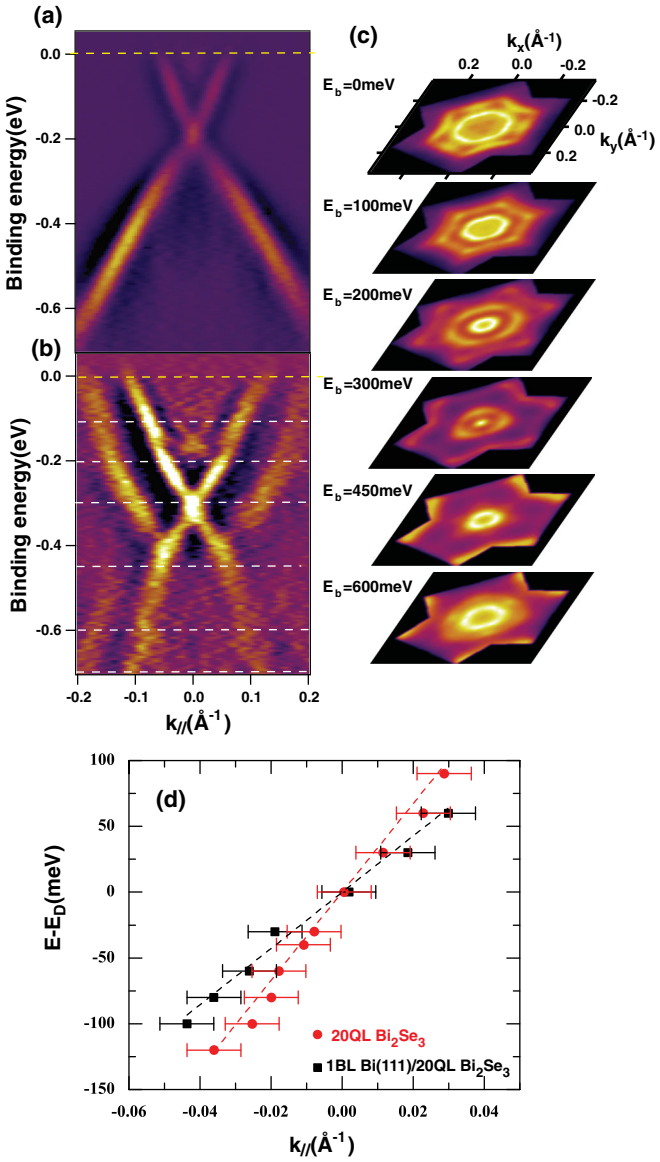

FIG. 4 (color online). (a) ARPES band map of 20 QL Bi_2Se_3. (b) ARPES band map and (c) constant energy contours of the Dirac surface states of 1 BL Bi(111)/20 QL Bi_2Se_3 heterostructure. All the spectra were taken along the $\bar{\Gamma}$-$\bar{K}$ direction at room temperature. (d) Comparison of Dirac surface states momentum vector of 20 QL Bi_2Se_3 and 1 BL Bi(111)/20 QL Bi_2Se_3. The dashed line is the fitting curve, whose slope indicates the Fermi group velocity of Dirac surface states in 20 QL Bi_2Se_3 and 1 BL Bi(111)/20 QL Bi_2Se_3.

in other words, the Fermi group velocity of Dirac fermions near DP is changed. Now the binding energy referred to the position of DP in each DSS of 20 QL Bi_2Se_3 at different certain momentum vectors is plotted and fitted using a proportional function in Fig. 4(d). The slope of the fitting line indicates the Fermi group velocity of the Dirac fermion of each DSS. The fitted Fermi group velocity of DSS in 1 BL Bi(111)/20 QL Bi_2Se_3 is $v_F \sim 3.24 \times 10^5$ m/s, but that in 20 QL Bi_2Se_3 is $v_F \sim 5.09 \times 10^5$ m/s. A 1 BL Bi(111) on the surface provides an additional degree of freedom to engineer DSS in TIs.

In order to further understand the physical origin of the unusual band structures, we performed the scanning tunneling microscopy (STM) measurements and DFT calculations to identify the configuration of Bi_2Se_3 thin film covered by 1 BL Bi(111). By delicate control of the Bi(111) growth condition, we were able to achieve BL-by-BL growth [14]. Figures 5(a) and 5(b) show the STM images of 1 BL Bi(111) and 0.5 BL Bi(111) on 20 QL Bi_2Se_3, respectively. Atomically flat morphology and sharp 1×1 reflection high-energy electron diffraction patterns [19] demonstrate the BL-by-BL growth mode and the high crystal quality of BL Bi(111); moiré patterns with the period ~4.57 nm can be seen in high resolution STM images [Fig. 5(b)], which originates from the in-plane lattice constant mismatch between Bi(111) (~4.54 Å) and Bi_2Se_3 (~4.13 Å). The simulated geometric structure of this heterostructure is shown in Fig. 5(c), where moiré patterns can also be observed. We choose three typical configurations (hereafter simplified as AB^1, AB^2, and AA stacking respectively) as prototypes to study their corresponding electronic structures via the DFT method, whose calculated electronic structures are shown in Figs. 5(d)–5(f). Compared with one another, we can find some common features in all three configurations: (i) a large Rashba splitting can be observed for the bands which are mainly contributed by the inserted 1 BL Bi(111) layer and hybridize with bulk states of substrate along the $\bar{\Gamma}$-$\bar{M}$ and $\bar{\Gamma}$-$\bar{K}$ directions; (ii) due to the inversion symmetry breaking, a Dirac cone [D_r shown in Figs. 5(d)–5(f)] from Rashba splitting of one BL Bi(111) coexists with the DSS of Bi_2Se_3 [D_s shown in Figs. 5(d)–5(f)], these results are consistent with the experiments and the previous report [16–18]; (iii) from the Bader analysis [27], it is found that some electrons transfer from the covered BL Bi(111) layer to the Bi_2Se_3 thin films, and just like the observation *in situ* ARPES, the sample is electron doped; (iv) in contrast to the unhybridized DSS located on the bottom surface, the DSS on the top surface is modified with reduced Fermi group velocity, which originates from the strong hybridization between the Bi(111) BL and top DSS of Bi_2Se_3 thin film.

Another interesting discovery on the 1 BL Bi(111)/20 QL Bi_2Se_3 heterostructure is the FSs via ARPES. To provide the insight, we analyze the contribution of the calculated states around the DSS on the top surface [dashed line in Fig. 5(f)], and plot their calculated FSs and related spin textures on experimental FSs in Fig. 4(c). As shown in Fig. 5(g), three calculated Bloch states in FSs are consistent with the experimental observation. The inner red one originates from the large Rashba splitting of Bi(111) BL, because the plotted FS is under D_r, the helicity of the spin texture is right handed [18]. The two cyan Bloch states are mainly contributed by the top DSS of Bi_2Se_3 film, the inner circle is the electronlike state with left-handed helicity spin texture, and the outer hexagonal one is the holelike state with the right-handed helicity spin texture but its energy dispersion has been strongly modified by the surface hybridization which also enhances its hexagonal warping effect [Fig. 5(g)]. The experimental FS of Rashba-like subbands is above D_r [see in Fig. 4(c)],

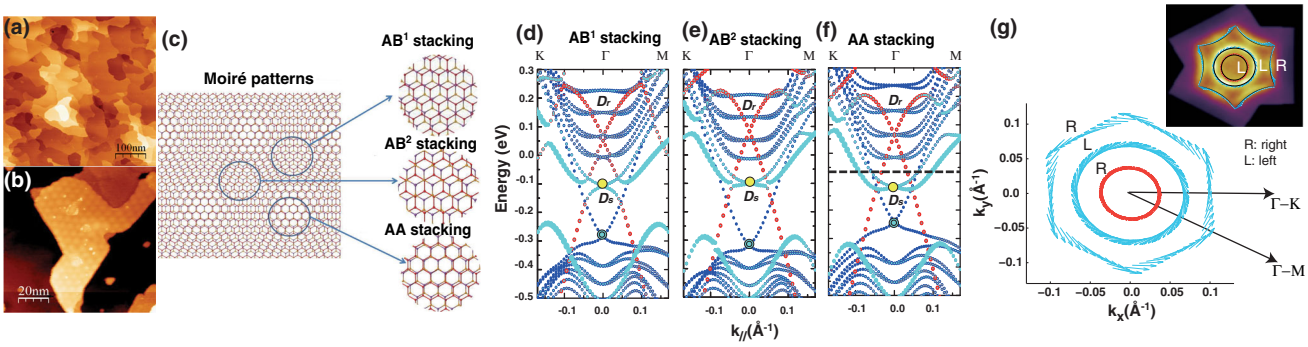

FIG. 5 (color online). (a) STM images of 500 nm × 500 nm taken from 1 BL Bi(111)/20 QL Bi_2Se_3 film. (b) High resolution STM images of 100 nm × 100 nm taken from 0.5 BL Bi(111)/20 QL Bi_2Se_3 film, moiré patterns can be observed. (c) Simulated moiré patterns for 1 BL Bi(111) on top of Bi_2Se_3 films, and the schematic diagrams of the stacking pattern are shown on the left, including AB^1, AB^2, and AA stacking. (d)–(f) The corresponding calculated band structures. Fermi levels are set to zero. The top and bottom DSSs of 6 QL Bi_2Se_3 are marked by the yellow and blue dots, respectively. The red and cyan solid dots in the band structures stand for the contribution of the top 1 BL Bi(111) and topmost 1 QL of Bi_2Se_3, respectively. (g) In-plane spin-momentum relationship of the constant energy contour whose energy is marked by the dashed line in (d) and spin texture of the experimental Fermi surface in 1 BL Bi(111)/20 QL Bi_2Se_3. The arrows indicate the spin direction, R means right-handed helicity, L means left-handed helicity.

and the helicity of the spin texture should be left handed, and, therefore, an alternating right-left-left helicity for the spin of consecutive FS of Rashba-like subbands and DSS is introduced, as shown in the top right corner of Fig. 5(g). Owing to the similar spin-momentum locking behavior between the red circular and the hexagonal Bloch states, we expect that the spin-dependent charge density wave could be observed in this system.

In summary, combined with *in situ* ARPES experiments and DFT calculations, we demonstrate that the DSS of 3D TI could be artificially engineered via van der Waals heterostructure growth of the cover layers. For the heterostructures deposited by one QL TI_c, the thin films are still topologically nontrivial, but the properties of the DSS, such as band dispersion and surface carrier type, can be engineered through the top cover layers. Moreover, because of the change of surface carrier type from the top to the bottom, a topological *p-n* junction naturally formed along the horizontal direction of the heterostructure; such a pairing of *p* and *n* type on opposite surfaces is likely to give rise to a topological exciton condensate with novel properties [28]. In addition, for 1 BL Bi(111) on Bi_2Se_3 thin films, the strong surface hybridization will not influence the coexistence of two DPs—one is from the strong Rashba splitting of topmost Bi BL and the other is the DSS of the Bi_2Se_3 top surface—but can reconstruct their spin-polarized FS. This work provides a method for artificially and independently engineering the DSS, and paves the way to design new TI materials for future spintronics and quantum computations.

We thank J. S. Moodera and M. D. Li for helpful discussions, and S. L. He and X. J. Zhou for the help in the generation of the FS. This work was supported by the National Natural Science Foundation of China, the ministry of Science and Technology of China, and the Chinese Academy of Sciences.

*Corresponding author.
czchang@mit.edu
†Corresponding author.
dwh@phys.tsinghua.edu.cn
‡Corresponding author.
kehe@mail.tsinghua.edu.cn

[1] M. Z. Hasan and C. L. Kane, Rev. Mod. Phys. **82**, 3045 (2010).
[2] X. L. Qi and S. C. Zhang, Rev. Mod. Phys. **83**, 1057 (2011).
[3] H. J. Zhang, C. X. Liu, X. L. Qi, X. Dai, Z. Fang, and S.-C. Zhang, Nat. Phys. **5**, 438 (2009).
[4] Y. Xia, D. Qian, D. Hsieh *et al.*, Nat. Phys. **5**, 398 (2009).
[5] Y. L. Chen *et al.*, Science **325**, 178 (2009).
[6] D. Hsieh *et al.*, Phys. Rev. Lett. **103**, 146401 (2009).
[7] R. Yu, W. Zhang, H. J. Zhang, S.-C. Zhang, X. Dai, and Z. Fang, Science **329**, 61 (2010).
[8] C. Z. Chang *et al.*, Science **340**, 167 (2013).
[9] C. Z. Chang, W. Zhao, D. Y. Kim, H. Zhang, B. A. Assaf, D. Heiman, S.-C. Zhang, C. Liu, M. H. W. Chan, and J. S. Moodera, Nat. Mater. **14**, 473 (2015).
[10] J. Zhang *et al.*, Nat. Commun. **2**, 574 (2011).
[11] D. S. Kong *et al.*, Nat. Nanotech. **6**, 705 (2011).
[12] Y. F. Zhao *et al.*, Sci. Rep. **3**, 3060 (2013).
[13] Y. Zhang, K. He, C. Z. Chang *et al.*, Nat. Phys. **6**, 584 (2010).
[14] M. Chen, J.-P. Peng, H.-M. Zhang, L.-L. Wang, K. He, X.-C. Ma, and Q.-K. Xue, Appl. Phys. Lett. **101**, 081603 (2012).
[15] Y. Y. Li *et al.*, Adv. Mater. **22**, 4002 (2010).
[16] T. Hirahara, G. Bihlmayer, Y. Sakamoto, M. Yamada, H. Miyazaki, S.-i. Kimura, S. Blügel, and S. Hasegawa, Phys. Rev. Lett. **107**, 166801 (2011).
[17] T. Hirahara *et al.*, Phys. Rev. Lett. **109**, 227401 (2012).
[18] L. Miao *et al.*, Proc. Natl. Acad. Sci. U.S.A. **110**, 2758 (2013).
[19] See Supplemental Material at http://link.aps.org/supplemental/10.1103/PhysRevLett.115.136801 for the detailed information of the ARPES measurements, the method of DFT calculations, and other supporting data, which includes Refs. [20–26].
[20] G. Kresse and J. Furthmuller, Phys. Rev. B **54**, 11169 (1996).
[21] P. E. Blochl, Phys. Rev. B **50**, 17953 (1994).
[22] J. P. Perdew, K. Burke, and M. Ernzerhof, Phys. Rev. Lett. **77**, 3865 (1996).
[23] S. Grimme, J. Antony, S. Ehrlich, and H. Krieg, J. Chem. Phys. **132**, 154104 (2010).
[24] P. Villars and L. D. Calvert, *Pearsons Handbook of Crystallographic Data for Intermetallic Phases* 2nd ed. (ASM International, Materials Park, OH, 1991).
[25] J. Neugebauer and M. Scheffler, Phys. Rev. B **46**, 16067 (1992).
[26] D. Hobbs, G. Kresse, and J. Hafner, Phys. Rev. B **62**, 11556 (2000).
[27] W. Tang, E. Sanville, and G. Henkelman, J. Phys. Condens. Matter **21**, 084204 (2009).
[28] B. Seradieh, J. E. Moore, and M. Franz, Phys. Rev. Lett. **103**, 066402 (2009).